NASA Technical Memorandum 101486

Acoustic Wave Propagation in Heterogeneous Structures Including Experimental Validation

Kenneth J. Baumeister and Milo D. Dahl
Lewis Research Center
Cleveland, Ohio

Prepared for the
12th Aeroacoustics Conference
sponsored by the American Institute of Aeronautics and Astronautics
San Antonio, Texas, April 10–12, 1989

NASA

ACOUSTIC WAVE PROPAGATION IN HETEROGENEOUS STRUCTURES INCLUDING EXPERIMENTAL VALIDATION

Kenneth J. Baumeister and Milo D. Dahl
National Aeronautics and Space Administration
Lewis Research Center
Cleveland, Ohio 44135

Abstract

A finite element model was developed to solve for the acoustic pressure and energy fields in a heterogeneous suppressor. The derivations from the governing equations assumed that the material properties could vary with position resulting in a heterogeneous variable property two-dimensional wave equation. This eliminated the necessity of finding the boundary conditions between different materials. For a two media region consisting of part air and part bulk absorber, a model was used to describe the bulk absorber properties in two directions. Complex metallic structures inside the air duct are simulated by simply changing element properties from air to the structural material in a pattern to describe the desired shapes. To verify the numerical theory, experiments were conducted without flow in a rectangular duct with a single folded cavity mounted above the duct and absorbing material mounted inside a cavity. Changes in a nearly plane wave sound field were measured on the wall opposite the absorbing cavity. Fairly good agreement was found in the standing wave pattern upstream of the absorber and in the decay of pressure level opposite the absorber, as a function of distance along the duct. The finite element model provides a convenient method for evaluating the acoustic properties of bulk absorbers.

Introduction

The Helmholtz resonator cavity, wall mounted bulk fibrous absorber and folded cavities are some of the most common means used to attenuate sound. Typical lining materials and construction techniques are shown in Fig. 1. The chief difference between the locally reacting liner and the extended reacting liners of Fig. 1 is illustrated in Fig. 2. In the locally reacting liner, such as the Helmholtz resonator shown in Fig. 2(a), the energy moves normal to the liner and depends only on the local value of acoustic pressure in the adjacent acoustic field. In contrast, the bulk extended reaction liner or the folded cavity, permits wave propagation in the axial direction, as shown in Fig. 2(b) and its attenuation characteristics can depend on the entire acoustic field.

Numerical techniques have been commonly employed in the study of mufflers and aircraft suppressors.[1,2] In general, the absorbing characteristics of the duct walls were modeled by applying the classical admittance boundary conditions at the duct walls. Consequently, wave propagation in the axial direction within the liner was generally not considered. In Ref. 3, a finite element theory was developed to model wave propagation in bulk materials as well as in any heterogeneous medium. The absorbing characteristics of the bulk material used in Ref. 3 relied on the theoretical development presented by Hersh in Ref. 4.

The present investigation will extend the work of Ref. 3 to account for termination reflections that occur from the exit in typical experiments and to determine the energy distribution around bulk absorber so that its effectiveness can be more accurately evaluated. The new experimental aspects of this paper will include more complex geometries for the code validation. In particular, advanced subsonic aircraft propulsion systems,[5] such as the ducted propeller shown in Fig. 3, employ thin cowls which may require the use of novel suppression techniques, such as folded cavities, to obtain low frequency sound suppression. As pointed out by Beckemeyer and Sawdy,[6] sound transmission characteristics can not be accurately predicted when local reactive impedance models are used. A folded cavity experiment is included as part of the new and more extensive validation of the heterogeneous finite element theory.

In the present paper, first the geometric model and the appropriate governing equations and boundary conditions will be presented. Next, the finite element procedure for modeling and solving complex problems will be discussed. Then a numerical solution and an analytical solution to a test problem will be compared. Finally, the results of three validation experiments will be discussed and compared to theory. New emphasis will be placed on following the energy propagation throughout the acoustic field.

Nomenclature

A	amplitude
A_n^+	amplitude of + going n entrance mode
A_n^-	amplitude of reflected - going n entrance mode
B_n^+	amplitude of + going n exit mode
B_n^-	amplitude of reflected - going n exit mode
b'	characteristic duct height
b_a	dimensionless entrance height b'_a/b'
b_b	dimensionless exit height b'_b/b'
c	dimensionless local speed of sound, c'/c'_o
c_e	dimensionless effective speed of sound, Eq. (2), c'_e/c'_o
c_o	dimensionless speed of sound (identical to unity)
c'_o	reference adiabatic speed of sound

E Property tensor, Eq. (10)

f' frequency

i $\sqrt{-1}$

K dimensionless heat transfer parameter, Eq. (2)

k wave number, Eq. (15)

k_{xn} axial modal wave number, Eqs. (13) and (14)

L dimensionless length, L'/b'

L_T position of exit reflection coefficient measurement

N_m number of modes in expansion, Eqs. (12) and (16)

n mode number, Eq. (12) or (16)

$\bar{n}$ unit outward normal, Eq. (28)

P dimensionless pressure, $P'(x,y,t)/\rho_o' c_o'^2$

p dimensionless pressure, $P(x,y,t)/e^{i\omega t}$

R_r exit reflection coefficient, Eq. (19)

t time

u dimensionless axial acoustic velocity, u'/c_{oa}'

x dimensionless axial distance coordinate, x'/b'

y dimensionless transverse distance coordinate, y'/b'

Z exit impedance, Eq. (18)

α exit reflection gradient correction, Eq. (24)

Γ exit reflection pressure correction, Eq. (22)

γ specific heat ratio

ϵ property constant, Eqs. (5) and (6)

ζ porosity

μ property constant, Eq. (7)

ρ dimensionless density, ρ'/ρ_o'

σ dimensionless viscous loss coefficient

ω dimensionless angular velocity, $\omega' b_a'/c_o'$

ω' angular velocity

Subscripts:

1 region 1

2 region 2

a entrance duct

b exit duct

i nodal point

o incident wave or ambient condition

x direction component

y direction component

Superscripts:

' dimensional quantity

~ approximate finite element prediction

Geometric Model

Consider the idealized acoustic duct shown in Fig. 4 which could be used to simulate acoustic wave propagation in a general duct in the absence of flow. The interior passage of the duct is assumed to contain air while a fibrous absorber is mounted in the cavity above the duct in the central portion. The lower wall is assumed hard or can be taken as a line of symmetry.

Some sort of acoustic pressure disturbance is assumed to generate a harmonic pressure field at minus infinity in the entrance duct. This field will propagate down the duct and act as the input driving boundary condition for the problem. A positive going acoustic wave of known magnitude is assumed at the entrance ($x = 0.0$) of the finite element portion of the duct. The pressure wave may be plane or have significant transverse y pressure variations. The present paper will focus on the interaction (absorption) of these propagating acoustic waves with the fibrous bulk absorbing material.

In the uniform, infinitely long entrance and exit section regions with perfectly hard walls, the exact solution of the governing differential equations can be easily written in terms of the duct modes; thus, simple analytical expressions can be employed to describe the pressure field in these regions. In the central region which includes both the duct and the fibrous absorbing region, the finite element analysis is employed to determine the pressure field.

The assumed known pressure waves propagating down the hard entrance duct are either reflected, transmitted or absorbed by the nonuniform segment of the duct containing the bulk absorber. Pressure mode reflection at the inlet to the absorbing region and transmission at the outlet of the absorbing region, are determined by matching the finite element solution in the interior of the central region to the known analytical eigen function expansions in the uniform inlet and outlet ducts. This permits a multimodal representation accounting for reflection and mode conversion by the nonuniform absorbing section. This approach has been found to accurately model reflection and transmission coefficients.[7]

Governing Equations

The governing equations are the state, continuity, and momentum linearized gas dynamics equations in the absence of mean flow. In the fibrous material, the Hersh form of the governing equations[4] will be employed. By treating the bulk material as a momentum and thermal sink, Hersh modified the conventional linearized gas equations

such that new complex propagation constants could account for acoustic energy absorption in the material. The development was semi-empirical since adjustable constants were employed; however, the dimensional parameters developed appear to accurately follow the experimental trends. Different sets of constants were determined for the fibers oriented perpendicular to, or parallel to, the direction of propagation. Consequently, some properties in the following equations will be subscripted with either x or y to indicate anisotropic behavior.

As shown in Ref. 3, the equations of state, continuity, and momentum were combined to yield the following wave equation in dimensionless form:

$$\frac{\partial}{\partial x}\left[\frac{1}{\left(\frac{\rho_o}{\zeta}+\frac{\sigma_x}{\zeta i\omega}\right)}\frac{\partial P}{\partial x}\right]+\frac{\partial}{\partial y}\left[\frac{1}{\left(\frac{\rho_o}{\zeta}+\frac{\sigma_y}{\zeta i\omega}\right)}\frac{\partial P}{\partial y}\right]-\frac{\zeta}{\rho_o c_e^2}\frac{\partial P^2}{\partial t^2}=0 \qquad (1)$$

The usual symbols for acoustic propagation are employed and all are explicitly defined in the Nomenclature. Some new terms that are not found in the conventional wave equation in air are the porosity ζ, viscous loss coefficient σ, and effective speed of sound c_e. The effective speed of sound is defined as

$$c_e^2=\frac{\partial P}{\partial \rho}=\frac{c_o^2}{\gamma}\left[\frac{\left(\frac{K}{\rho_o\omega}\right)+i\gamma}{\left(\frac{K}{\rho_o\omega}\right)+i}\right] \qquad (2)$$

where K represents a dimensionless heat transfer parameter defined in Ref. 3 or 4 in relation to the physical properties of the bulk absorber. For high frequencies, $K/\rho_o\omega \ll 1$, the usual adiabatic relationship for the speed of sound is recovered.

Assuming the pressure perturbation P to be harmonic in time,

$$P(x,y,t)=p(x,y)e^{i\omega t} \qquad (3)$$

Eq. (1) becomes

$$\frac{\partial}{\partial x}\left[\frac{1}{\left(\frac{\rho_o}{\zeta}-\frac{i\sigma_x}{\zeta\omega}\right)}\frac{\partial p}{\partial x}\right]+\frac{\partial}{\partial y}\left[\frac{1}{\left(\frac{\rho_o}{\zeta}-\frac{i\sigma_y}{\zeta\omega}\right)}\right]\frac{\partial p}{\partial y}+\frac{\zeta\omega^2}{\rho_o c_e^2}p=0 \qquad (4)$$

For simplicity, let

$$\varepsilon_x=\frac{\rho_o}{\zeta}-i\frac{\sigma_x}{\zeta\omega} \qquad (5)$$

$$\varepsilon_y=\frac{\rho_o}{\zeta}-i\frac{\sigma_y}{\zeta\omega} \qquad (6)$$

$$\mu=\frac{\zeta}{\rho_o c_e^2} \qquad (7)$$

Thus, the wave equation becomes

$$\frac{\partial}{\partial x}\left(\frac{1}{\varepsilon_x}\frac{\partial p}{\partial x}\right)+\frac{\partial}{\partial y}\left(\frac{1}{\varepsilon_y}\frac{\partial p}{\partial y}\right)+\mu\omega^2 p=0 \qquad (8)$$

Equation (8) represents the governing wave equation to be solved by finite element theory.

For later use in applying the finite element theory, it is convenient to express Eq. (8) in vector form,

$$\nabla\cdot(\bar{E}\cdot\nabla p)+\mu\omega^2 p=0 \qquad (9)$$

where the property tensor $\bar{E}$ is represented by

$$\bar{E}=\begin{pmatrix}\frac{1}{\varepsilon_x} & 0\\ 0 & \frac{1}{\varepsilon_y}\end{pmatrix} \qquad (10)$$

and the vector product of the tensor $\bar{E}$ and a vector ∇p follows the common definition (Eqs. (A.4-19), Ref. 8).

Uniform Duct Analytical Solution

The proper termination boundary condition of the finite element region requires that acoustic waves are not artificially reflected by the numerical difference equations employed at the first or last column of nodal points. Considerable research has been expended in the acoustic and electromagnetic fields to obtain a good numerical approximation for this condition. Using this research base, the analytical solution of Eq. (8) for acoustic wave propagation in a uniform hard wall duct will be employed to give the termination boundary condition for the finite element region.

The analytical solution for pressure waves traveling between parallel hard plates where the boundary condition is

$$\frac{\partial p}{\partial y}=0 \quad \text{at} \quad y=0 \quad \text{and} \quad y=b_a \qquad (11)$$

is given as (see for example Ref. 9, p. 504)

$$p_a(x,y)=\sum_{n=1}^{N_m}A_n^+\cos\left[\frac{(n-1)\pi}{b_a}y\right]e^{-ik_{xn}x}+\sum_{n=1}^{N_m}A_n^-\cos\left[\frac{(n-1)\pi}{b_a}y\right]e^{+ik_{xn}x} \qquad (12)$$

For the $e^{i\omega t}$ time dependence used here, the $A_n^+e^{-ik_{xn}x}$ term represents a wave propagating in

the positive x direction while the $A_n^- e^{ik_{xn}x}$ term represents a wave moving in the negative x direction.

The axial wave number k_{xn} in Eq. (12) is

$$k_{xn} = k\sqrt{1 - \left[\frac{(n-1)\pi}{b_a k}\right]^2} \qquad \frac{(n-1)\pi}{b_a k} \leq 1 \tag{13}$$

$$k_{xn} = -ik\left|\sqrt{\left[\frac{(n-1)\pi}{b_a k}\right]^2 - 1}\right| \qquad \frac{(n-1)\pi}{b_a k} > 1 \tag{14}$$

$$k = \omega\sqrt{\mu\varepsilon} = \frac{\omega}{c_o} \tag{15}$$

The modal expression represented by Eq. (12) has been truncated to a total of N_m modes of the infinite number possible. Thus, a total of N_m unknown modal amplitudes A_1^-, A_2^-, -- A_{Nm}^- have been introduced. The A^+ terms will be assumed as known. N_m constraint equations will be required to determine each of these unknown reflection coefficients. The equations used to define these coefficients will be introduced in the following section on boundary conditions.

A similar solution exists at the exit, except only positive going waves are considered

$$p_b(x,y) = \sum_{n=1}^{N_m} B_n^+ \cos\left[\frac{(n-1)\pi}{b_b} y\right] e^{-ik_{xn}x} \tag{16}$$

where k_{xn} in Eq. (16) is based on characteristic duct height of exit b_b.

Unfortunately, in a real world experiment duct apparatus, reflections occur at the termination of the duct. In many cases, absorptive material is included in the termination to reduce this reflection. The reflections are observed in the experimental data by the appearance of small standing wave patterns at the duct exit. From these standing wave patterns or other means[10] the impedance or exit reflection coefficient can be measured. For plane wave propagation, Eq. (16) can be modified to account for exit reflection. Since only a single plane wave approximation to Eq. (16) will be considered, the finite element grid must be extended sufficiently far from the exit so that all higher order modes decay. This is easily checked by examining contour pressure plots of the acoustic field.

For a single plane wave propagating in the exit duct, Eq. (16) can be rewritten as

$$p(x) = B_1^+ e^{-ikx} + B_1^- e^{ikx} = B_1^+ e^{-ikx}\left[1 + \frac{B_1^-}{B_1^+} e^{i2kx}\right] \tag{17}$$

In this case, the reflected wave represented by the B^- term has been included in the propagation equation. The impedance at any x value is defined as

$$\frac{Z(x)}{\rho_o c_o} = \frac{p}{\rho_o c_o u} = \frac{p}{\frac{c_o i}{\omega}\frac{\partial p}{\partial x}} = \frac{1 + \frac{B_1^-}{B_1^+} e^{i2kx}}{1 - \frac{B_1^-}{B_1^+} e^{i2kx}} \tag{18}$$

or

$$\frac{B_1^-}{B_1^+} = \frac{\frac{Z(x)}{\rho_o c_o} - 1}{\frac{Z(x)}{\rho_o c_o} + 1} e^{-i2kx} = R_r(x)e^{-i2kx} = \text{constant} \tag{19}$$

If the measured value of the exit impedance or reflection coefficient is taken at position L_T it follows that

$$\frac{B_1^-}{B_1^+} = R_r(L_T)e^{-i2kL_T} \tag{20}$$

Substituting Eq. (20) back into Eq. (17) yields the new pressure requirement at the exit

$$p(x) = \Gamma B_1^+ e^{-ikx} \tag{21}$$

where

$$\Gamma = 1 + R_r(L_T)e^{-i2k(L_T - x)} \tag{22}$$

In a similar manner, the new condition for the pressure gradient at the exit, which is used in the finite element formulation, can be written as

$$\frac{\partial p}{\partial x} = -ik\alpha B_1^+ e^{-jkx} \tag{23}$$

where

$$\alpha = 1 - R_r(L_T)e^{-i2k(L_T - x)} \tag{24}$$

Boundary Conditions

A variety of boundary conditions will be used in the finite element solution of Eq. (1) for the model problem which is displayed in Fig. 4. Each of the conditions will now be briefly discussed.

Input Conditions

The analysis assumes a given number of N_m positive going waves whose amplitudes A_n^+ are known. These modes effectively set the level of the scalar pressure field in the finite element region and can be viewed as the equivalent Dirichlet boundary conditions required for the elliptic boundary value problem defined by Eq. (1).

In all the solutions to be presented in the results section of this report, a plane wave input is assumed; that is, A_1^+ is taken as unity and the rest of the higher modal amplitudes are assumed zero.

Pressure Continuity

In general, the scalar pressure field is continuous across an interface except where sources are present. Thus, the boundary condition at the interface between the entrance duct and the finite element region requires

$$p_a = \tilde{p} \quad (x = 0;\ 0 < y < b_a) \tag{25}$$

where p_a is the modal representation of the scalar pressure field in the analytical inlet region given by Eq. (12) and $\tilde{p}$ implies an approximate finite element numerical solution to the true solution. Applying Eq. (25) is not quite as easy as it looks. A weighted residual approach is used with the weighting function equal to the eigen function of the analytical solution represented by the cosine terms in Eq. (12). N_m separate equations are generated; one for each of the unknown reflection coefficients. A full discussion can be found in Ref. 10, Eqs. (43) to (52). Similar equations are used at the exit.

Velocity Continuity

In addition to the pressure continuity, the axial acoustic velocity must also be continuous across the interface to the finite element region.

$$u_a = \tilde{u} \quad (x = 0;\ 0 < y < b_a) \tag{26}$$

Again, u_a is the modal representation of the axial velocity field in the analytical solution and $\tilde{u}$ represents the approximate finite element solution. Using the momentum equations (Ref. 3, Eq. (21)) to express the axial velocity in terms of the pressure field yields

$$\frac{1}{\rho_a}\frac{\partial p_a}{\partial x} = \frac{1}{\varepsilon_x}\frac{\partial \tilde{p}}{\partial x} \tag{27}$$

Again, a similar equation applies at the exit.

Hard Wall Boundary Condition

At the hard walls shown in Fig. 4, the transverse acoustic velocity is zero. Again, using the momentum equations to relate the acoustic velocity to the pressure fields requires

$$\nabla p \cdot \bar{n} = 0 \tag{28}$$

Finite Element Theory

The finite element formulation of the heterogeneous wave equation is now generated by using the weighted residual approach with the Galerkin approximation to obtain an integral form of the variable property wave equation over the whole (global) domain.

The continuous domain D is first divided into a number of discrete areas as shown in Fig. 4. The particular pattern chosen has been found to give accurate results for a minimum number of elements.[12]

In the classical weighted residual manner, the pressure field is curve-fitted in terms of all the unknown nodal values $p_i(x_i, y_i)$. The finite element aspects of converting Eq. (1) and the boundary conditions into an appropriate set of global difference equations can be found in text books[13] as well as in Ref. 11 and for conciseness will not be presented herein. In Ref. 11, an exact finite element analog of Eq. (1) for electromagnetic propagation has been solved by the Galerkin finite element theory with linear elements.

Experimental Apparatus and Procedure

A test apparatus was constructed to verify the numerical method for a duct having a fibrous absorbing wall and no mean flow. The general acoustic duct system described in Ref. 3 was employed. The simple no-flow apparatus is shown schematically in Fig. 5 while an actual photograph of the test section and instrumentation is shown in Fig. 6. The experimental system was designed to simulate plane wave propagation in an infinite duct.

Reference 3 describes in detail the acoustic source, test section, fibrous absorber test sample, microphone installation, and measurement accuracy. The particular configuration used in the tests will be described in the Discussion of Results section which now follows.

Discussion of Results

For theory and code validation, the finite element solution is first applied to a theoretical case where an exact analytical solution exists. Next, the experimental results are compared to finite element predictions.

Normal Incidence

The first case considers a step change in material density from a nondimensional value of 1 to a value of 4 at an axial position of x equals 0.25 inside the finite element grid, as seen in the upper portion of Fig. 7. In this case the porosity is unity, and the viscous loss coefficients σ_x and σ_y are assumed to be zero so that ε_x and ε_y take on the real values of 1 and 4, respectively. The μ parameter was assumed to be 1 and the dimensionless incident frequency was assumed to be 2π.

As shown in Fig. 7, the finite element and exact analytical theories (Ref. 14, p. 83) are in excellent agreement for the rms pressure. The reflections from the interface between the two density changes are clearly represented by the standing wave pattern ahead of the interface. Observe that the magnitude of the pressure increases inside the material.

The key facet of this example illustrates that it is not necessary to employ any interfacial boundary conditions. The change in properties at the interface is automatically handled by the heterogeneous form of the differential equation. As seen in Fig. 7, the change in material at x of 0.25 inside the finite element grid automatically produces the reflected standing wave characteristic of an impedance change.

Wall Absorber

Figure 8 shows a comparison of experiment to theory for the open bulk absorber case shown by the upper schematic in Fig. 8 and by the actual hardware in Fig. 6. In the theoretical predictions, the material properties were evaluated using Hersh's correlations.[4] However, a parametric evaluation of Hersh's viscous loss coefficient indicated that increasing the viscous loss parameter would improve the correlation of the experimental results. Consequently, Hersh's prediction for the viscous loss coefficient was increased from 0.1133 to 0.4133. Other experimental observations also suggested that Hersh's empirical coefficient σ could be underestimating viscous effects. Using an impedance tube, Dahl and Rice[10] reported larger measured absorption than predicted with the Hersh model in the 1500 Hz frequency range associated with the present experiment. The following properties were used in the experimental data correlation:

$P_r = 0.71$ $\quad \nu' = 1.51\times10^{-5}$ m^2/sec $\quad f' = 1560$ Hz

$\gamma = 1.4$ $\quad d' = 1.254\times10^{-5}$ m $\quad V_p = 1.0$

$V_n = 0.44$ $\quad Tn = 1.0$ $\quad \zeta = 0.9945$ (29)

and

$$\varepsilon_x = \varepsilon_y = 1.0055 - i0.4133 \quad (30)$$

$$\mu = 1.0000 - i0.04805 \quad (31)$$

The exit termination reflection coefficient $R_r(L_T)$ used in Eq. (20) was measured. Using this measured value of $R_r(L_T)$, Γ and α in Eqs. (22) and (24) were calculated as follows:

$$\Gamma(L_T) = 0.9176 + i0.0977 \quad (32)$$

$$\alpha(L_T) = 1.0824 - i0.0977 \quad (33)$$

As seen in Fig. 8, the theory and experiment are in good agreement. In particular, the magnitude and wave length of the entrance standing wave due to the bulk absorber cavity is in close agreement with theory although a slight shift in the pattern (phase) is seen. The fall off of pressure in the central portion of the duct is also predicted very well. In the axial region from x equals 8 to 12 as shown in Fig. 8, the standing wave pattern results from reflections off the absorbing wedge in the exit horn (see Fig. 5). The theory very accurately predicts these standing waves.

The theory used to predict the standing wave patterns in the exit assumed a single dominant plane wave. Since the first nonplane mode begins propagating at a frequency of 1701 Hz in the experimental apparatus of Fig. 6, the choice of 1560 Hz for the data frequency guarantees that only plane waves will propagate in the straight portion of the duct far from the fibrous absorption area. This is clearly shown by the theoretical contour plots shown in Fig. 9. In the vicinity of the fibrous bulk absorber entrance and exit region, higher order acoustic modes are present as indicated by the nonplanar pressure profiles. However, far from the bulk absorber region at the axial position of x equals 13, where the analytical region couples to the finite element region, the pressure wave profile is essentially plane. Thus the plane wave reflection coefficient theory of Eq. (17) is valid.

Finally, the theory can be used to evaluate the local effectiveness of a bulk absorber by determining the axial acoustic energy content of the duct. The energy at any axial position is the transverse summation of the local acoustic intensity (product of pressure p and conjugate acoustic velocity u) across the duct. Figure 10 displays the axial energy as a function of axial position for this experimental case. The incoming wave energy has been normalized to a value of 1. Thus, the dip in incoming energy below 1 in the entrance portion of the duct represents the reflected component of energy. Surprisingly, at the axial position of 7 to 8, the net energy in the duct is rising. Energy entering the beginning portion of the bulk absorber is transported through the absorber to the exit portion of the duct. Thus, the second half of the bulk absorber is very ineffective in reducing the transmitted energy.

Folded Cavity

Folded cavities have been found to be useful in the reduction of low frequency sound in confined spaces such as turbofan nacelles[5] or in the thin cowl of the high speed ducted propellers shown in Fig. 3. Low frequency noise suppression in these aircraft cowls can be achieved without excessive acoustic liner backing depth if the backing volume is formed as a long shallow cavity folded to lie along the length of the cowl.

The second experiment and theory comparison will illustrate how easily the finite element theory can be modified to account for complex absorbing cavities in the wall. In particular, a folded cavity was constructed by "taping over" a portion of the bulk absorber interface thus creating a folded cavity (see the upper portion of Fig. 11).

To model this folded cavity, the same finite element grid is employed in the solution as was used in Fig. 8. However, in this case, the material properties representing the metal tape were simulated by simply changing the real part of ε to a large number (1×10^9). In effect a large impedance mismatch is generated at the interface so that these elements now represent the solid metallic surface of the tape.

As seen in Fig. 11, the theory and experiment are still in good agreement. The magnitude of the standing wave in the entrance duct is somewhat larger than the previous case but still in reasonable agreement with the theory. The fall off of pressure in the central portion of the duct is still predicted quite accurately. A second analysis was also performed with the elements shown in insert A of Fig. 11 with identical results. In this case, the element thickness was equal to the thickness of the tape and appears as a solid line in insert A.

Finally, the energy level in the folded cavity experiment was found to decrease throughout the duct as shown in Fig. 12. In this case the final energy level at the exit termination was slightly less than the previous example shown in Fig. 10. Part of this decrease is due to increased reflected energy at the entrance of the folded cavity.

Structural Blockage

To simulate blockage in a duct or tunnel with splitters or instrumentation support, two metallic spacers were inserted into the test duct as shown by the upper schematic of Fig. 13. Again, this structure was simulated merely by changing the properties of the elements in the duct as was done with the folded cavity. Thus, the same finite element grid was employed in the solution. As with the previous two cases, good agreement between the theory and experiment is seen in Fig. 13.

Concluding Remarks

A finite element model was developed to solve for the acoustic pressure field in a region that was heterogeneous. The derivation from the governing equations assumed no mean flow and that the material properties could vary with position resulting in a heterogeneous variable property two-dimensional wave equation. This eliminated the necessity of finding the boundary conditions between the different materials. Consequently, complex structures can be easily modeled simply by changing the properties of elements in the calculational domain.

For a two media region consisting of part air and part bulk absorber, a model was used to describe the bulk absorber properties in two directions. Experiments to verify the numerical theory were conducted in a rectangular duct with no mean flow, absorbing material mounted on one wall, and various forms of structure introduced into the duct. Changes in the sound field, consisting of planar waves, were measured on the wall opposite the absorbing material. As a function of distance along the duct, fairly good agreement was found in the standing wave pattern upstream of the absorber and in the decay of pressure level opposite the absorber.

The numerical formulation is relatively simple to use and appears to give accurate modeling of the experimental data. The theory may be a useful tool in the evaluation of viscous loss coefficients in bulk materials.

References

1. Baumeister, K.J., "Numerical Techniques in Linear Duct Acoustics - A Status Report," Journal of Engineering for Industry, Vol. 103, No. 3, Aug. 1981, pp. 270-281.

2. Baumeister, K.J., "Numerical Techniques in Linear Duct Acoustics - 1980-81 Update," NASA TM-82730, 1981.

3. Baumeister, K.J. and Dahl, M.D., "A Finite Element Model for Wave Propagation in an Inhomogeneous Material Including Experimental Validation," AIAA Paper 87-2741, Oct. 1987 (also, NASA TM-100149).

4. Hersh, A.S. and Walker, B., "Acoustic Behavior of Fibrous Bulk Materials," AIAA Paper 80-0986, June 1980.

5. Groeneweg, J.F. and Bober, J.L., "Advanced Propeller Research," Aeropopulsion 87, Session 5: Subsonic Propulsion Technology," NASA CP-10003, 1987, pp. 5-123 to 5-152.

6. Beckemeyer, R.J. and Sawdy, D.T., "Analytical and Experimental Studies of Folded Cavity Duct Acoustic Liners," Paper presented at 92nd Meeting of the Acoustical Society of America, San Diego, CA, Nov. 16-19, 1976.

7. Baummeister, K.J., Eversman, W., Astley, R.J., and White, J.W., "Acoustics in Variable Area Duct: Finite Element and Finite Difference Comparisons to Experiment," AIAA Journal, Vol. 21, No. 2, Feb. 1983, pp. 193-199.

8. Bird, R.B., Stewart, W.E., and Lightfoot, E.N., Transport Phenomena, John Wiley and Sons, New York, 1960.

9. Morse, P.M. and Ingard, K.U., Theoretical Acoustics, McGraw-Hill, New York, 1968.

10. Dahl, M.D. and Rice, E.J., "Measured Acoustic Properties of Variable and Low Density Bulk Absorbers," ASME Paper 85-WA/NCA-6, Nov. 1985 (also, NASA TM-87065).

11. Baumeister, K.J., "Finite Element Analysis of Electromagnetic Propagation in an Absorbing Wave Guide," NASA TM-88866, 1986.

12. Baumeister, K.J., "Effect of Triangular Element Orientation on Finite Element Solutions of the Helmholtz Equation," NASA TM-87351, 1986.

13. Sergerlind, L.J., Applied Finite Element Analysis, John Wiley & Sons, New York, 1976.

14. Temkins, S., Elements of Acoustics, John Wiley and Sons, 1981.

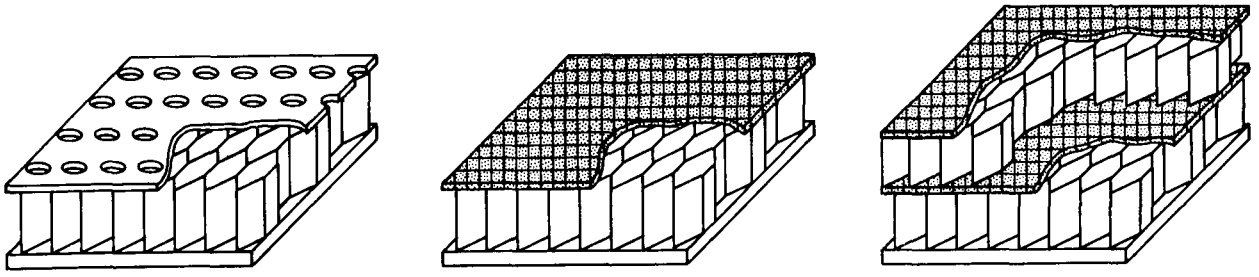

(a) LOCAL REACTION LINERS.

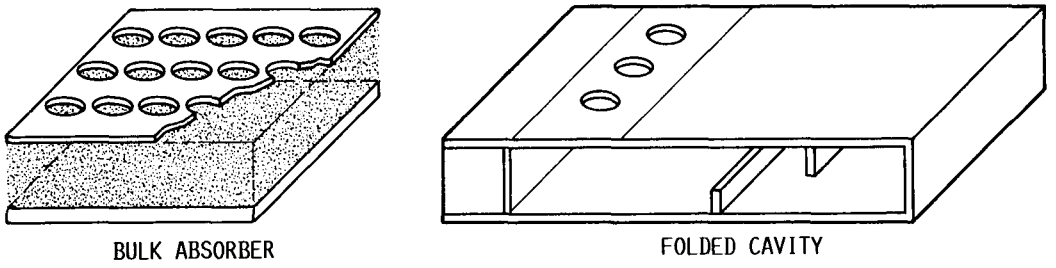

(b) EXTENDED REACTION LINERS.

FIGURE 1. - LINING MATERIALS AND CONSTRUCTION.

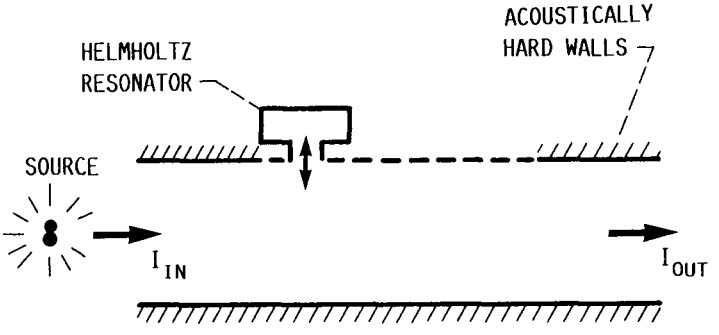

(a) LOCALLY REACTING ABSORBING ADMITTANCE BOUNDARY CONDITION.

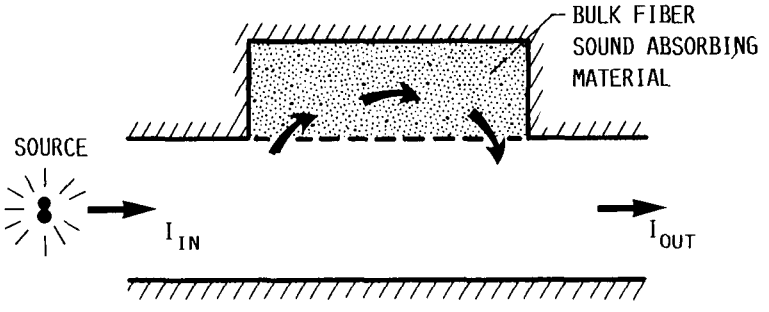

(b) EXTENDED REACTING INHOMOGENEOUS ABSORBING BOUNDARY.

FIGURE 2. - BOUNDARY CONDITIONS EMPLOYED TO SIMULATED ABSORBING WALL.

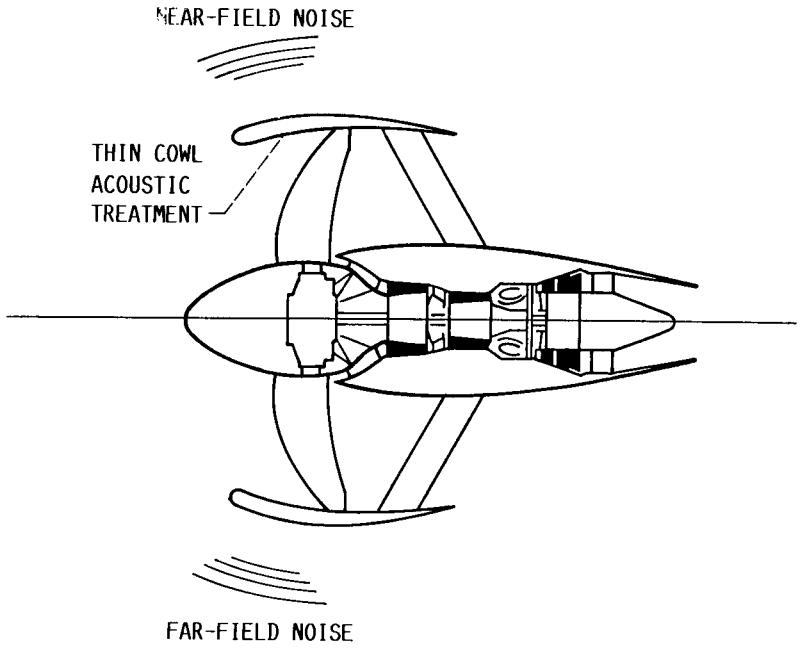

FIGURE 3. - HIGH-SPEED DUCTED PROPELLER ACOUSTICS.

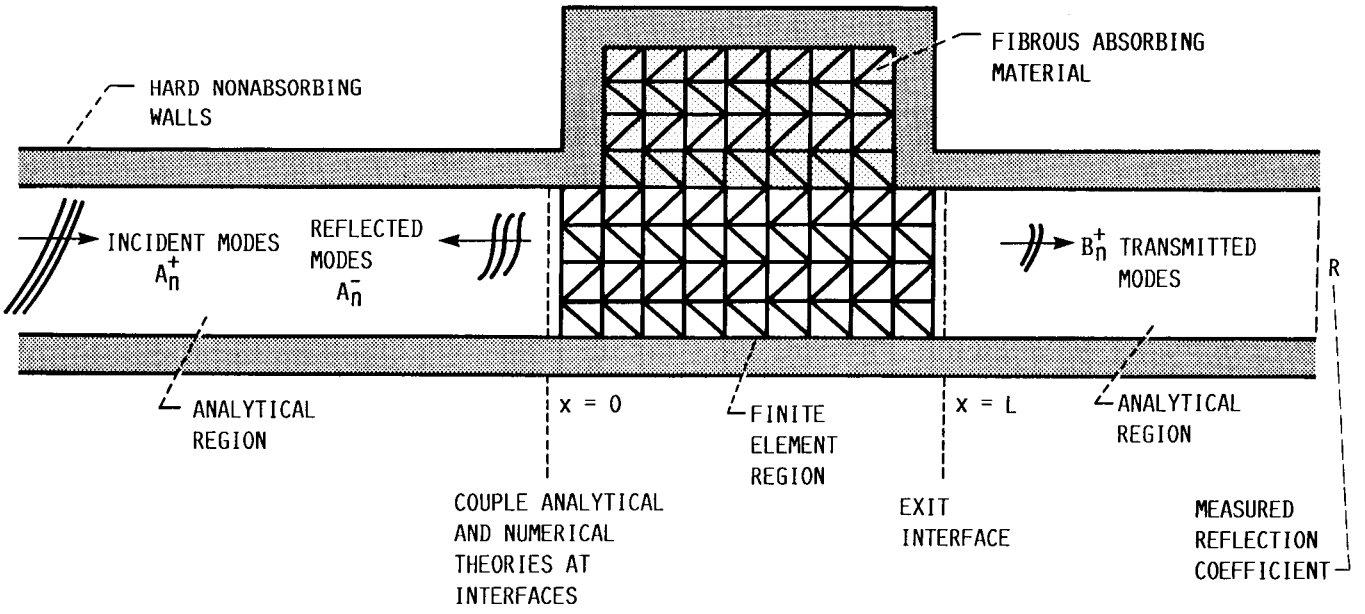

FIGURE 4. - TWO DIMENSIONAL DUCT FINITE ELEMENT MODEL.

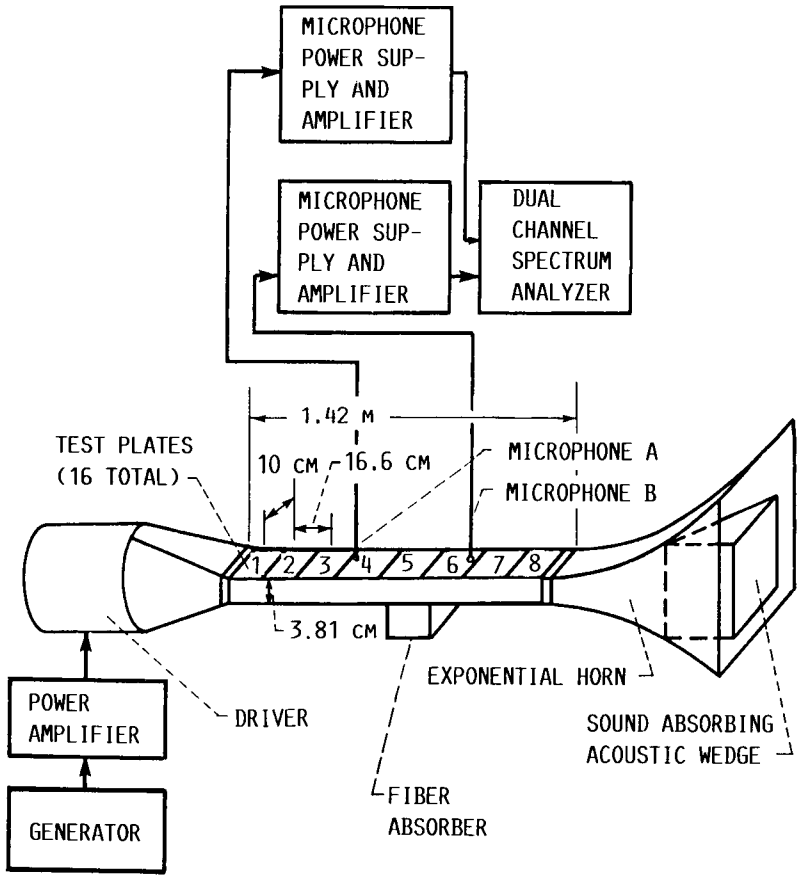

FIGURE 5. - NO-FLOW ACOUSTIC DUCT TEST SECTION AND INSTRUMENTATION.

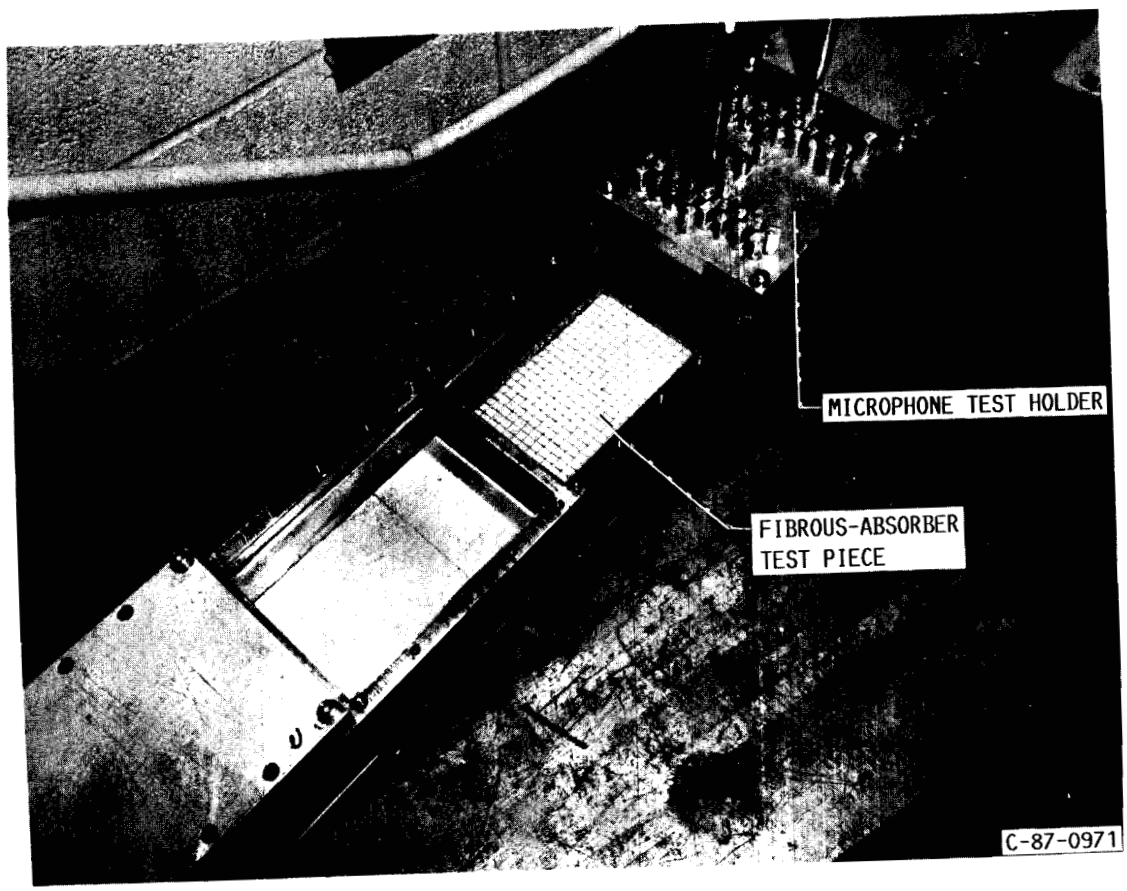

FIGURE 6. - MICROPHONE TEST PLATE AND MOUNTED FIBROUS ABSORBER.

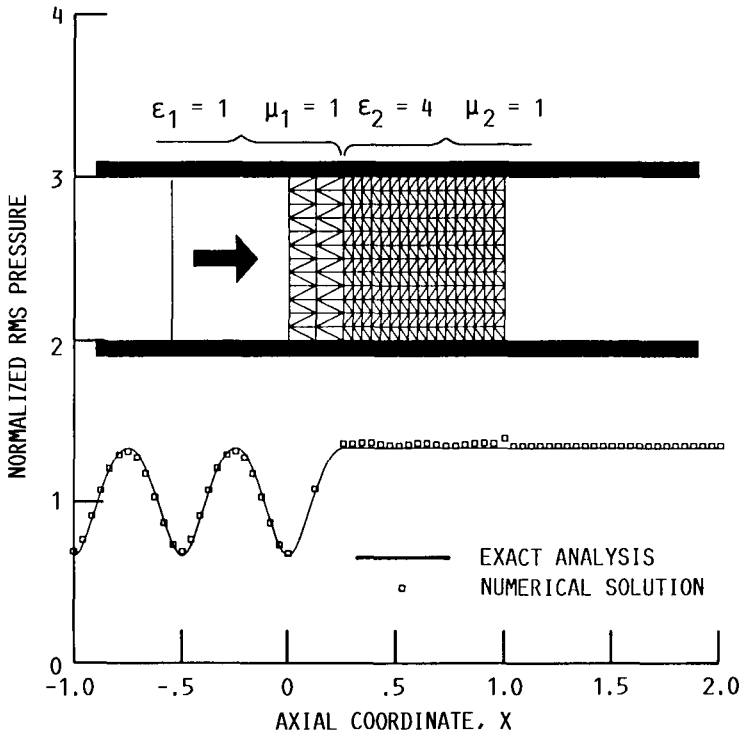

FIGURE 7. - COMPARISON OF THE MAGNITUDE OF THE AXIAL RMS PRESSURE VARIATION ALONG THE LOWER WALL IN A UNIFORM DUCT WITH HARD WALLS AND A CHANGE IN PROPERTIES OF THE MEDIA AT X OF 0.25 (ε_1 = 1.0 AND ε_2 = 4.0) AS OBTAINED BY USING AN EXACT SOLUTION AND A FINITE SOLUTION FOR A PLANE WAVE (MODE-ONE) INCIDENT AT X = 0 WITH $\omega = 2\pi$.

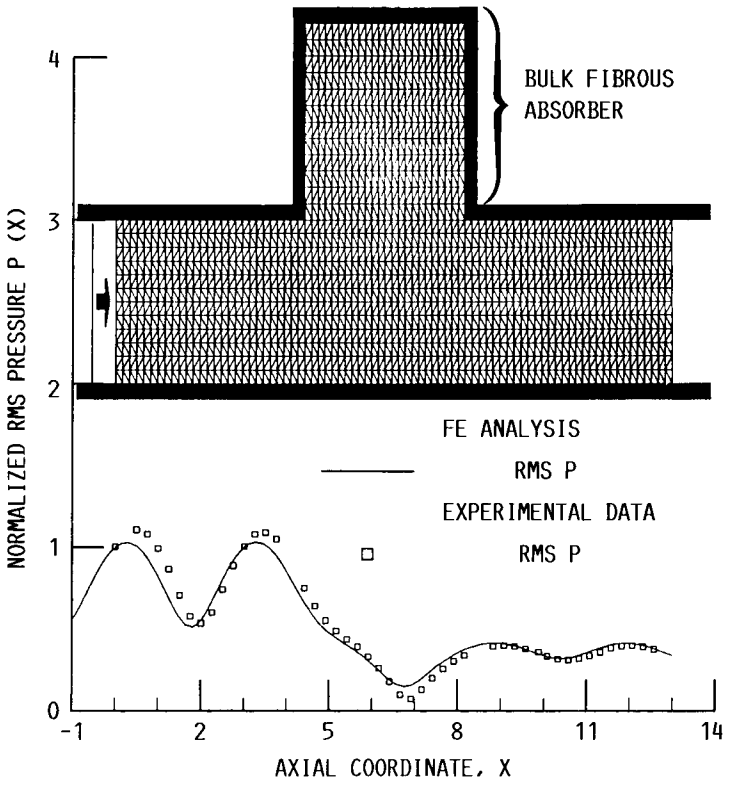

FIGURE 8. - EXPERIMENTAL AND THEORETICAL AXIAL PRESSURE PROFILE ALONG LOWER WALL FOR OPEN BULK CAVITY.

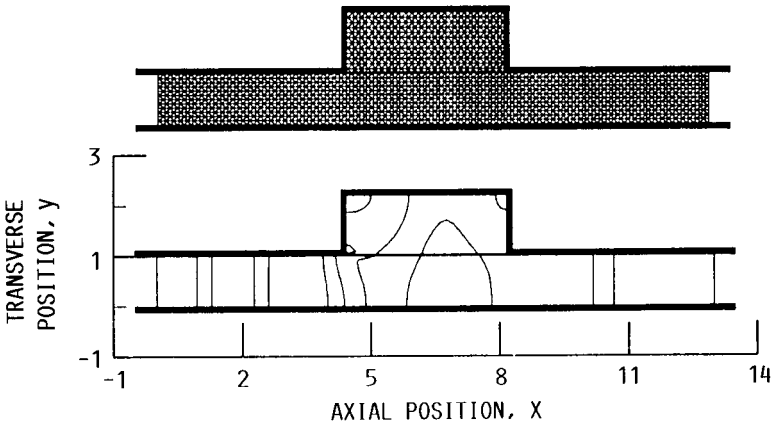

FIGURE 9. - CONTOUR PLOTS OF RMS PRESSURE AMPLITUDE FOR OPEN BULK CAVITY.

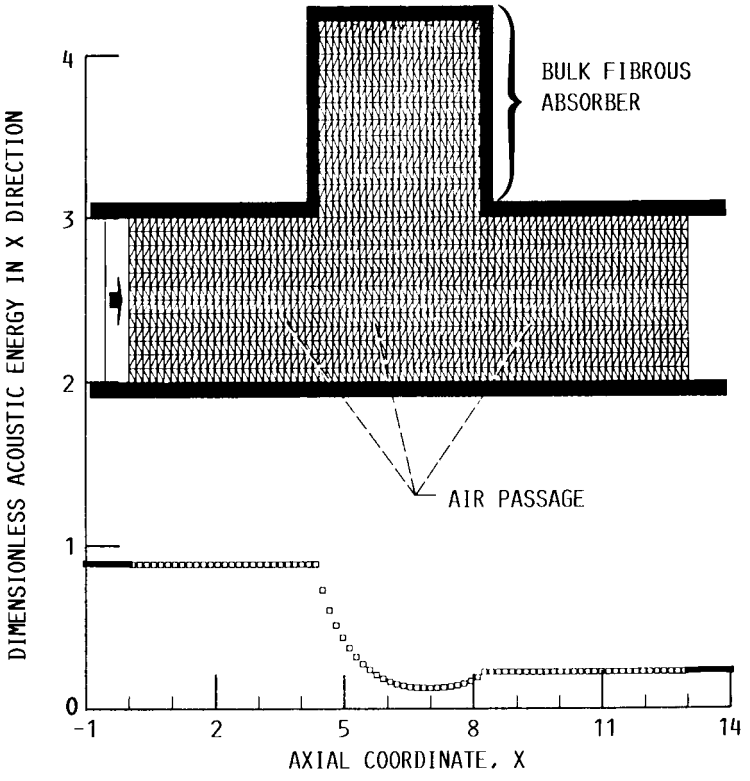

FIGURE 10. - AXIAL ACOUSTIC ENERGY IN THE AIR DUCT AS A FUNCTION OF AXIAL POSITION FOR OPEN BULK CAVITY.

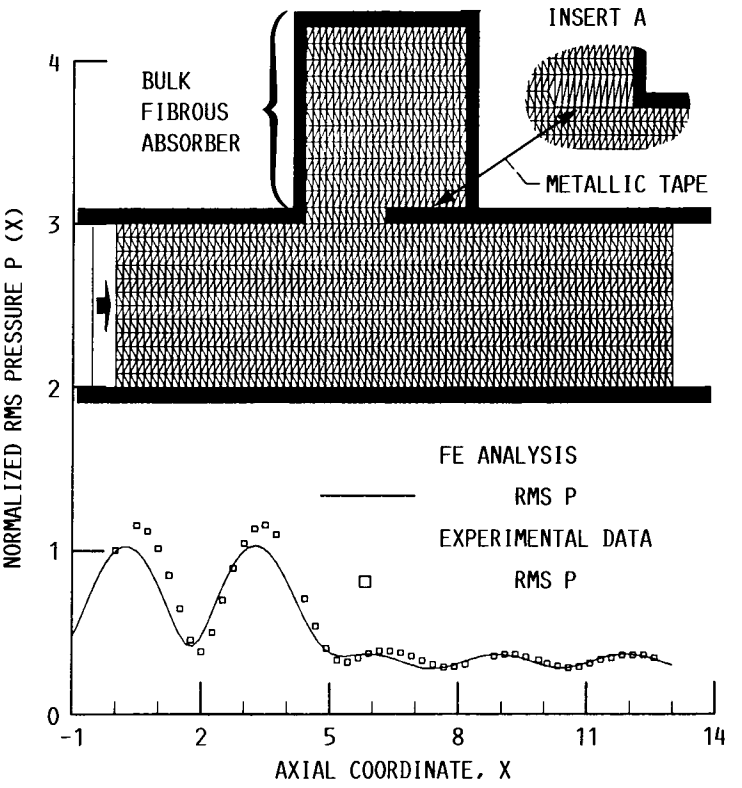

FIGURE 11. - EXPERIMENTAL AND THEORETICAL AXIAL PRESSURE PROFILE FOR FOLDED CAVITY BULK ABSORBER AS MEASURED ALONG THE LOWER WALL.

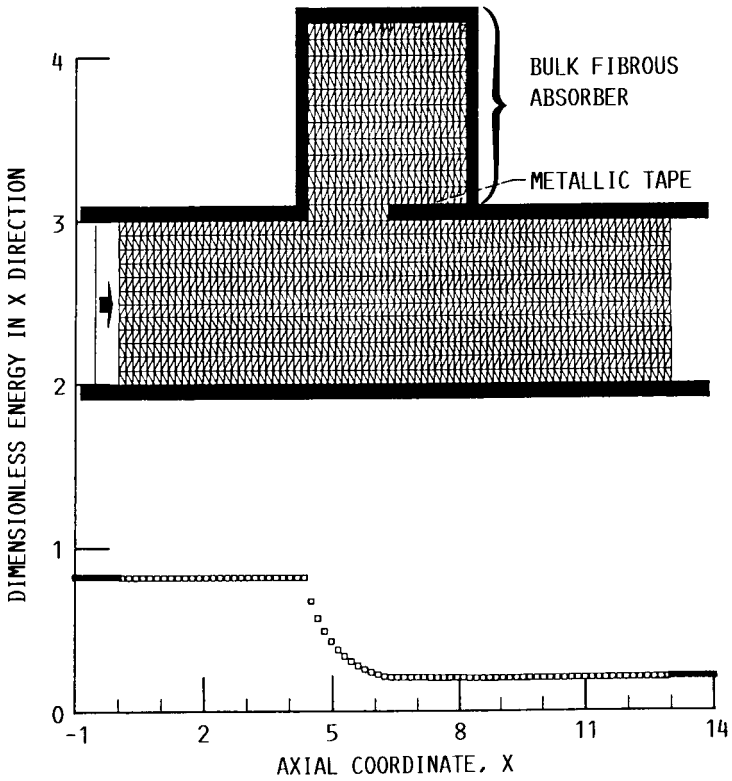

FIGURE 12. - AXIAL ACOUSTIC ENERGY IN THE AIR DUCT AS A FUNCTION OF AXIAL POSITION FOR THE FOLDED CAVITY BULK ABSORBER.

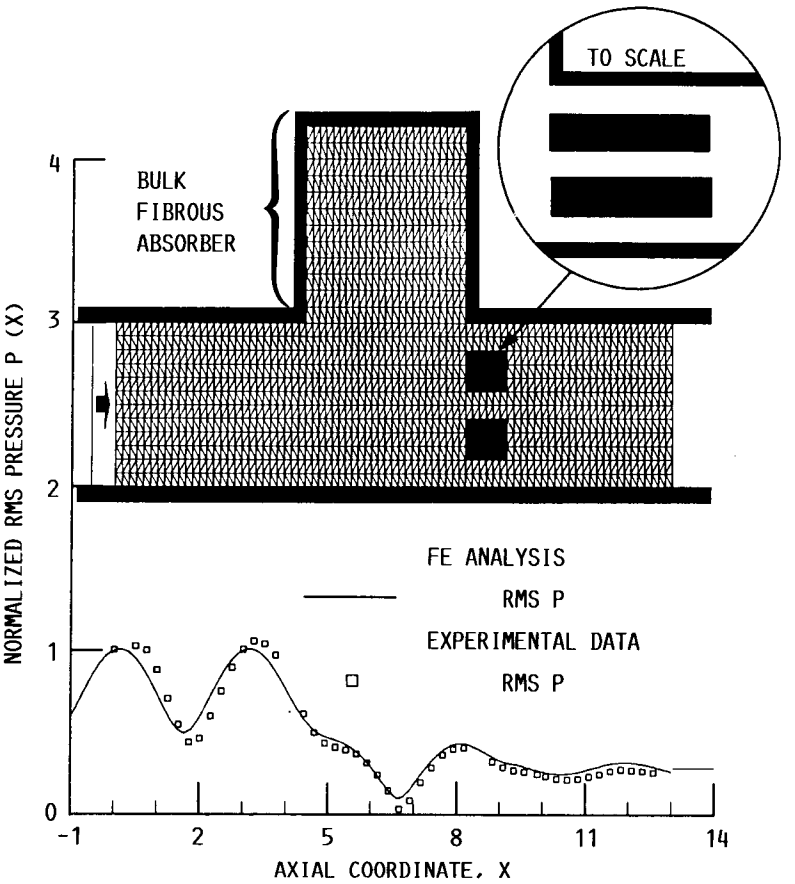

FIGURE 13. - EXPERIMENTAL AND THEORETICAL AXIAL PRESSURE PROFILES ALONG THE LOWER WALL FOR STRUCTURAL MATERIAL INSIDE THE DUCT.

NASA
National Aeronautics and Space Administration

Report Documentation Page

1. Report No.	2. Government Accession No.	3. Recipient's Catalog No.
NASA TM-101486		

4. Title and Subtitle	5. Report Date
Acoustic Wave Propagation in Heterogeneous Structures Including Experimental Validation	6. Performing Organization Code

7. Author(s)	8. Performing Organization Report No.
Kenneth J. Baumeister and Milo D. Dahl	E-4622
	10. Work Unit No. 505-62-21

9. Performing Organization Name and Address	11. Contract or Grant No.
National Aeronautics and Space Administration Lewis Research Center Cleveland, Ohio 44135-3191	13. Type of Report and Period Covered Technical Memorandum
12. Sponsoring Agency Name and Address	14. Sponsoring Agency Code
National Aeronautics and Space Administration Washington, D.C. 20546-0001	

15. Supplementary Notes

Prepared for the 12th Aeroacoustics Conference sponsored by the American Institute of Aeronautics and Astronautics, San Antonia, Texas, April 10-12, 1989.

16. Abstract

A finite element model was developed to solve for the acoustic pressure and energy fields in a heterogeneous suppressor. The derivations from the governing equations assumed that the material properties could vary with position resulting in a heterogeneous variable property two-dimensional wave equation. This eliminated the necessity of finding the boundary conditions between different materials. For a two media region consisting of part air and part bulk absorber, a model was used to describe the bulk absorber properties in two directions. Complex metallic structures inside the air duct are simulated by simply changing element properties from air to the structural material in a pattern to describe the desired shapes. To verify the numerical theory, experiments were conducted without flow in a rectangular duct with a single folded cavity mounted above the duct and absorbing material mounted inside a cavity. Changes in a nearly plane wave sound field were measured on the wall opposite the absorbing cavity. Fairly good agreement was found in the standing wave pattern upstream of the absorber and in the decay of pressure level opposite the absorber, as a function of distance along the duct. The finite element model provides a convenient method for evaluating the acoustic properties of bulk absorbers.

17. Key Words (Suggested by Author(s))	18. Distribution Statement
Acoustics Finite element Bulk absorbers Experimental data	Unclassified - Unlimited Subject Category 70

19. Security Classif. (of this report)	20. Security Classif. (of this page)	21. No of pages	22. Price*
Unclassified	Unclassified	18	A03

*For sale by the National Technical Information Service, Springfield, Virginia 22161